Immunosensor Enhanced with Silver Nanocrystals for On-Chip Prostate Specific Antigen Detection

Timothy Anton Okhai *, Kefilwe Vanessa Mokwebo, Marlon Oranzie, Usisipho Feleni, Lukas Willem Snyman

Posted Date: 20 May 2025

doi: 10.20944/preprints202505.1547.v1

Keywords: Biosensors; Cancer; Immunosensors, Nanomaterials; On-chip; Prostate Specific Antigen; Silver Nanocrystals

 doi:10.20944/preprints202505.1547.v1

Article

Immunosensor Enhanced with Silver Nanocrystals for On-Chip Prostate Specific Antigen Detection.

Timothy A. Okhai [1,2,*], Kefilwe V. Mokwebo [3], Marlon Oranzie [3], Usisipho Feleni [4] and Lukas W. Snyman [2]

[1] Clinical Engineering Group, Department of Electrical Engineering, Faculty of Engineering and the Built Environment, Tshwane University of Technology, Pretoria, South Africa

[2] Department of Electrical Engineering, College of Science, Engineering and Technology, University of South Africa, Florida Campus, South Africa; snymalw@tut.c.za

[3] SensorLab, Department of Chemistry, University of the Western Cape, Bellville 7535, South Africa; 3696304@myuwc.ac.za (K.V.M); 3338704@myuwc.ac.za (M.O)

[4] Institute for Nanotechnology and Water Sustainability (iNanoWS), Florida Campus, College of Science, Engineering and Technology, University of South Africa, Johannesburg 1710, South Africa; felenu@unisa.ac.za

* Correspondence: okhaita@tut.ac.za; Tel: +27 823 424 844

Abstract: An electrochemical immunosensor for the quantification of prostate specific antigens (PSA) using silver nanocrystals (AgNCs) is reported. The silver nanocrystals were synthesized using a conventional citrate reduction protocol. The silver nanocrystals were characterized using scanning electron microscopy (SEM) and field effect scanning electron microscopy (FESEM), x-ray diffraction (XRD), high-resolution transmission electron microscopy (HRTEM), Fourier transform infrared spectroscopy (FTIR), UV-Vis spectroscopy, and small angle X-ray scattering (SAXS). The proposed immunosensor was fabricated on a glassy carbon electrode (GCE) sequentially by drop-coating AgNCs, the electro-deposition of EDC-NHS, the immobilization of anti-PSA antibody (Ab), and dropping of bovine serum albumin (BSA) to prevent non-specific binding sites. Each stage of the fabrication process was characterized by cyclic voltammetry (CV). Using square wave voltammetry (SWV), the proposed immunosensor displayed high sensitivity in detecting PSA over a concentration range of 1 to 10 ng/mL with a detection limit of 1.14 ng/mL and R^2 of 0.99%. The immunosensor was selective in the presence of interfering substances like glucose, urea, L-cysteine, and alpha-methylacyl-CoA racemases (AMACR) and it showed good stability and repeatability. These results compare favourably with some previously reported results on similar or related technologies for PSA detection.

Keywords: biosensors; cancer**;** immunosensors; nanomaterials; on-chip; prostate specific antigen; silver nanocrystals

1. Introduction

The detection, monitoring and management of tumours in clinical medicine and oncology has been enhanced by recent advancements in the discovery of different tumour biomarkers. Among these biomarkers are alpha-fetoprotein (AFP), used to assess the baby's risk of birth abnormalities and genetic conditions such as Down syndrome and neutral tube defect during pregnancy; cytokeratin 19 fragment (cyfra 21-1), a serum marker for detecting lung cancer, esophageal cancer, head and neck cancer, anal canal cancer and gynaecological cancer, and cancer antigen-125 (CA125), an antigenic tumour marker that can diagnose or monitor ovarian, fallopian tube or primary peritoneal cancer. Others are carcinoembryonic antigen (CEA), a tumour biomarker linked with liver, colorectal, ovarian, breast and lung cancer, and prostate-specific antigen (PSA), the biomarker for

 doi:10.20944/preprints202505.1547.v1

detecting prostate cancer [1–3]. The most common cancer in males worldwide, which is prostate cancer, poses a significant health risk. Research indicates that the standard prostate-specific antigen (PSA) level in normal human serum is below 4 ng/mL, however, values over 20 ng/mL are frequently linked to the existence of prostate cancer [4–8]. Early detection of this disease is crucial for improving survival rates and treatment outcomes. This is typically accomplished by measuring PSA levels in the blood. The enzyme-linked immunosorbent assay (ELISA) is the standard method used in many clinical environments for PSA detection [9]. However, this approach has some drawbacks, including the setup cost, as it requires expensive laboratory equipment and skilled personnel, and the long processing time for the results, which can take several hours or days to process. Consequently, there is a pressing need for a detection method that addresses these limitations by offering a rapid, cost-effective, and user-friendly solution to enhance early detection and improve survival rates for prostate cancer patients.

Recent studies have explored various innovative detection tools for prostate-specific antigens to enhance the accuracy and specificity of prostate cancer diagnosis. [10,11] These advanced detection technologies include aptasensors, enzyme-based sensors, and immunosensors. Aptasensors utilize nucleic acid aptamers that bind specifically to PSA molecules, allowing for the detection of low concentrations of PSA in biological samples. They have high specificity and sensitivity and have been shown to achieve detection limits in the picomolar range. Their ease of use, rapid response time, and the possibility of integration into portable devices for point-of-care testing make them suitable for early diagnosis of prostate cancer [10]. Enzyme-based sensors typically involve immobilizing enzymes that catalyze reactions, producing measurable signals in the presence of PSA. For example, Oliveira et al. have explored using horseradish peroxidase (HRP) conjugate with anti-PSA antibodies to create a colorimetric assay that provides a visual indication of PSA levels [11]. This method is simple, cost-effective, and maintains adequate sensitivity for clinical applications. Immunosensors employ antibodies that specifically recognize PSA to provide quantitative measurements. They accomplish this by employing bovine serum albumin (BSA) to obstruct non-specific sites and concentrate exclusively on the specific sites of the antibodies, a process crucial for enhancing the specificity and accuracy of the sensor. When a sample containing PSA is introduced, the PSA molecules bind non-specifically to the capture antibodies. The blocked non-specific sites ensure that only PSA binds to the sensor, reducing background noise and improving the accuracy of the detection [12,13]. The change in the sensor's signal is proportional to the concentration of PSA in the sample. This allows for the quantitative measurement of PSA levels with very high sensitivity [13]. Recent advances in this field have focused on enhancing the sensitivity and selectivity of immunosensors by modifying them with various modifications, such as nanomaterials, to amplify the signals produced [14]. This work focuses on developing an electrochemical immunosensor that utilizes silver nanocrystals to significantly improve the detection limit. This facilitates PSA detection levels at concentrations much lower than traditional methods, potentially reducing false positives and unnecessary biopsies.

Silver nanoparticles significantly enhance the sensitivity of immunosensors through several mechanisms that leverage their unique chemical and physical properties. They have a high surface area relative to their volume, allowing for increased binding sites for target biomolecules [15]. Their signal amplification capabilities are due to their ability to dissolve in certain systems and to release silver ions (Ag^+), which can then interact with fluorescent probes or other signaling molecules to significantly amplify the detectable signals [16]. They exhibit excellent electrocatalytic properties, which improve the electrochemical response of immunosensors [15]. Their ability to facilitate electron transfer enhances the sensitivity of electrochemical detection methods, allowing for lower limits of detection compared to conventional techniques. The unique optical properties of silver nanoparticles enable surface plasmon resonance, which enhances the optical signals in biosensing applications [15]. Furthermore, the inherent antimicrobial properties of silver nanoparticles help maintain sensor performance by reducing contamination risks during assays [16]. Finally, their versatility in functionalization ensures that silver nanoparticles can be easily functionalized with various

 doi:10.20944/preprints202505.1547.v1

biomolecules (e.g., antibodies), allowing for tailored sensor designs that enhance specificity and sensitivity for particular targets [15]. This is crucial for developing highly specific immunosensors capable of detecting a wide range of biomarkers. These advantages make silver nanocrystals a valuable component in developing advanced biosensing technologies for clinical diagnosis and other applications requiring high sensitivity and specificity. In our previous research on nanomaterial-enhanced receptor technology for silicon on-chip biosensing applications [17,18], we demonstrated that both basic and sophisticated micro and nano sensors can be seamlessly integrated onto a silicon chip utilizing silicon avalanche mode light emitting devices (Si AMLEDs) and conventional silicon integrated circuit processing, capable of detecting various parameters through waveguide optics, evanescent fields, and waveguide-based receptor layers. It was also proposed that the selectivity and sensitivity of these biosensor devices may be improved by including a layer of nanomaterial within the receptor cavity. This article is an extension of that work, and the goal of this present work is to present a novel electrochemical immunosensor for the quantification of PSA using silver nanocrystals, with the potential for integration into a silicon photonic microchip for rapid deployment at a point of care.

2. Materials and Methods

2.1. Chemicals and Equipment

For the synthesis of the silver nanocrystals, the chemicals used were silver nitrate ($AgNO_3$ 99+ %), trisodium citrate dihydrate ($Na_3C_6H_5O_7$), sodium borohydride ($NaBH_4$, 98%), sodium chloride (NaCl), sodium bromide (NaBr, 98%), potassium iodide (KI) and ascorbic acid (AA). All these chemicals were purchased from Sigma Aldrich, South Africa, and were used as received. The chemicals used to prepare the immunosensor were monoclonal anti-PSA antibody, EDC-NHS, and BSA, all purchased from Sigma Aldrich. The PSA is of analytical grade and was also purchased from Sigma Aldrich. All glassware were cleaned with aqua regia (3:1 v/v HCl (37%)/HNO_3 (65%) solutions) and then rinsed thoroughly with H_2O before use. All experiments utilized Milli-Q water (18 MΩ cm, Millipore). Various analytical methods and tools were used to characterize the AgNCs. The JSM-7800F Field Emission Scanning Electron Microscope (FESEM) was used to examine the surface structure and elemental signature of the silver nanocrystals, paired with energy-dispersive X-ray spectroscopy (EDS). The functional groups were studied using the KBr pellet technique on a Frontier PerkinElmer Fourier transform infrared (FTIR) spectrometer (Spectrum 100 spectrometer) in the 400-4000 cm^{-1} wavelength region. To determine the particle size distributions, a transmission electron microscope model JEOL JSM 100 CX II was utilized, with the maximum voltage being set at 100 kV. GraphPad Prism® Version 5.03 was used to plot the TEM images and results. The PANanalysis XRD equipment and High Score software were used for the X-ray diffraction (XRD) analysis. Using Origin 2021 software, all of the data gathered from the characterization apparatus were plotted.

2.2. Synthesis of Silver Nanocrystals

A slightly modified technique adapted from Li et al. [19] was used to synthesize the AgNCs. The following protocol was followed in the synthesis of the AgNCs: This citrate reduction procedure involved dissolving 9 mg of $AgNO_3$ in 50 mL of H_2O and bringing it to a boil while stirring. The boiling $AgNO_3$ solution was then quickly mixed with 1 mL of a sodium citrate (1 wt %) aqueous solution while being vigorously stirred. As the reaction time increased, the reaction solution's colour altered from colourless to yellow to turbid and brown. To increase the production yield of AgNCs, the resulting brown solution was kept boiling while being stirred for an hour. After cooling to room temperature, the solution was kept at 4 °C until it was needed.

 doi:10.20944/preprints202505.1547.v1

2.3. Immunosensor Fabrication Process

Before being employed, the glassy carbon electrode (GCE) was meticulously polished to provide a smooth, consistent surface, and sonicated for 30 minutes. Each step of the immunosensor development process was characterized by cyclic voltammetry (CV). First, 5 mL of 10 mM phosphate buffer solution (PBS) of pH 7.4 was measured and poured into a glass vial with a three-electrode setup, i.e., the working electrode, the reference electrode, and a platinum wire counter electrode. Then, CV measurements were carried out on the bare GCE at a scan rate of 50 mV/s in the potential window of -1.0 to 1.0 V, and the measurement values were recorded for the bare GCE. Then, the GCE was modified with 10 µL (10 mg/mL) of AgNCs and left overnight to dry before the CV was repeated. This time, the measured values were labelled as GCE/AgNC. After gentle rinsing with deionized water and PBS, the electrode was modified with 1-ethyl-3-(3-dimethylaminopropyl) carbodiimide/N-hydroxy succinimide (EDC/NHS) cross-linking chemistries for 30 mins. at room temperature for activation of the amine groups to bind covalently to the carboxyl groups of the antibody. Next, 50 µL of (10 µg/mL) of the antibody (Ab) was drop-coated on the electrode and left to dry for 1 hour, forming the GCE|AgNC|Ab. Next, 20 µL of 1% BSA was drop-coated onto the electrode for 1 hour to block non-specific binding sites, forming the GCE|AgNC|Ab|BSA immunosensor. Each stage of the fabrication process was characterized by CV and SWV in 10 mM PBS (pH 7.4) at a scan rate of 50 mV/s in the potential window of -1.0 to 1.0 V. Finally, different concentrations of the PSA antigen were spiked into the electrochemical cell for detection via SWV. The fabricated immunosensor GCE|AgNC|Ab|BSA was refrigerated at 4 °C when not in use. Figure 1 is the schematic representation of the immunosensor fabrication process.

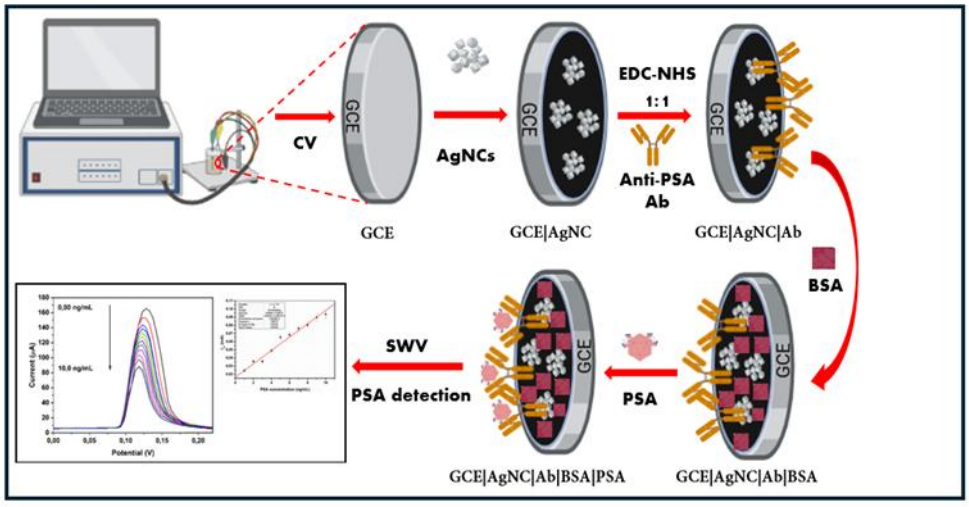

Figure 1. Schematic showing the immunosensor fabrication process.

2.4. Experimental Measurements

The experimental procedure involves electrochemical measurements performed on a three-electrode system in a glass vial. This consists of a platinum wire counter electrode, a reference electrode, and a 3 mm glassy carbon electrode (GCE), which serves as the working electrode. The experimental parameters for the CV measurements were an E-step of 5 mV, t-equilibration of 2 s, a current range of 1 mA, a scan rate of 50 mV/s, and a potential window of -1.0 to 1.0 V. The supporting electrolyte was 10 mM phosphate buffer solution (pH 7.4). A pulse duration of 10 ms, a pulse amplitude of 10 mV, a current of 1 µA, a scan rate of 50 mV/s, and an equilibration time of 5 s were the experimental settings for the differential pulse voltammetry (DPV). For the square wave voltammetry (SWV), the experimental parameters were a pulse amplitude of 25 mV, a current range of 1 µA, a scan rate of -1.0 to 1.0 V, an E-step of 5 mV, a frequency of 10 Hz, and a t-equilibration of 2 s.

 doi:10.20944/preprints202505.1547.v1

3. Results and Discussions

3.1. Characterization of Nanomaterials

Figures 2 (a) and (b) illustrate the scanning electron microscope (SEM) and field effect scanning electron microscope (FESEM) topographical images of the nanoparticles. These equipment were used to investigate the shape, size, impurities, and stability of the particles. The globular-shaped morphology of the AgNCs shown in the SEM image in Figure 2 is in line with what is anticipated for silver nanoparticles. During the nucleation and growth of silver nanocrystals from a solution or vapour phase, the atoms or ions arrange themselves to reduce the number of high-energy surface atoms, naturally leading to a globular (spherical or near-spherical) shape [20]. The globular morphology of AgNCs has several important implications for their properties and applications. Firstly, while a sphere minimizes surface area for a given volume, nanoparticles in general have a very high surface area to volume ratio compared to their bulk counterparts. Globular nanoparticles offer a significant surface area for interactions with their surroundings, which is crucial for applications like catalysis, sensing, and antimicrobial activity. Secondly, the catalytic activity of AgNCs is influenced by the number of active sites available on their surface, which is related to their surface area and the specific crystal facets exposed. Thirdly, silver nanoparticles are well-known for their antimicrobial properties, and the high surface area of globular nanoparticles facilitates these interactions. Finally, the collective oscillation of silver nanoparticles' conduction electrons in response to incident light gives them distinctive optical characteristics. The size and shape of the nanoparticles have a significant impact on this phenomenon, which is called surface plasmon resonance (SPR). Globular silver nanoparticles typically exhibit a single SPR band in the visible region of the electromagnetic spectrum, in contrast with non-spherical shapes that can have multiple SPR bands at different wavelengths, leading to different colours and optical properties that are advantageous for certain applications like biosensing. It is therefore often necessary to employ various synthesis strategies and capping agents to control the morphology of AgNCs and tailor their properties for specific applications like biosensing [21].

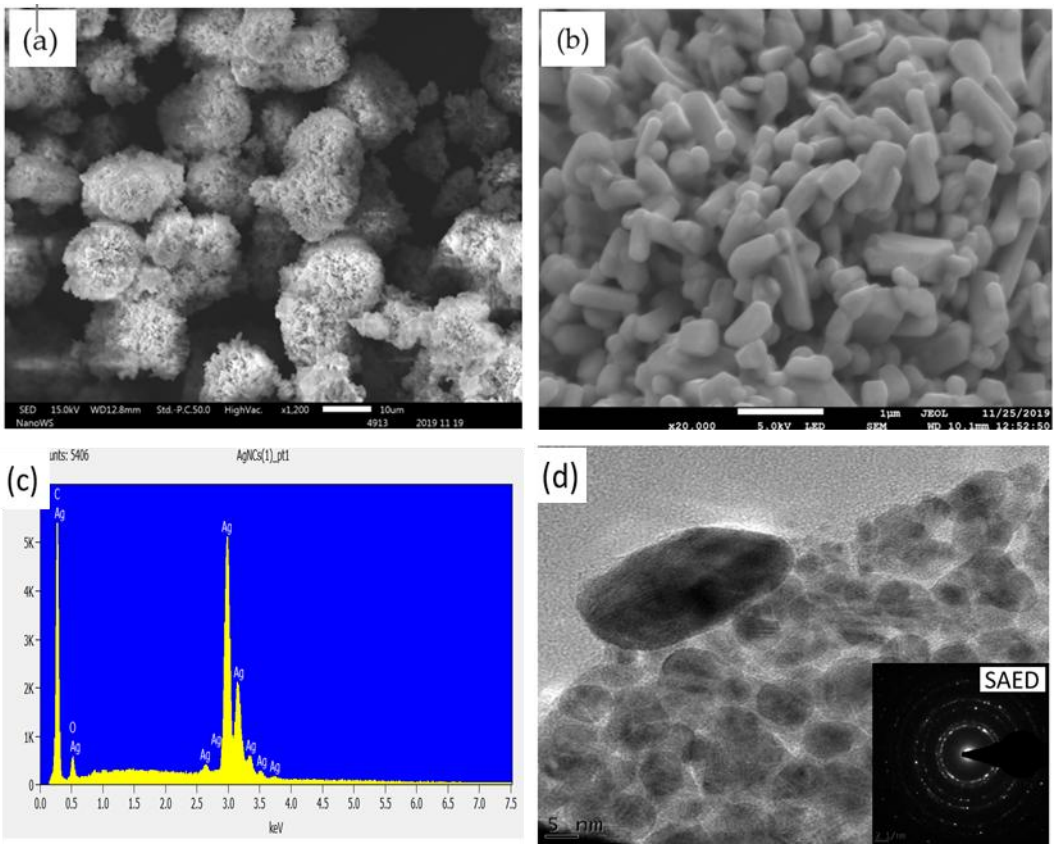

 doi:10.20944/preprints202505.1547.v1

Figure 2. (a) SEM photomicrograph at x1200, (b) FE-SEM photomicrograph at x10,000, (c) energy dispersion X-ray spectroscopy graph, and (d) transmission electron microscopy image.

The FE-SEM image in Figure 2 (b) shows a unique capsule-like shape which somewhat appears close to nanotablets, with the dimensions measuring between 227 nm and 471 nm in width, and between 770 nm and 1.64 μm in length (average 1.21 μm). Energy dispersion X-ray spectroscopy (EDS) was used to determine the elemental composition of the AgNCs, as illustrated in Figure 2 (c). The EDS analysis confirms that silver is the predominant element detected. The morphology of the AgNCs is consistent with what is expected for silver nanoparticles. From the TEM image in Figure 2 (d), most of the particles appear at 1.7 nm radius, with a maximum diameter of 17 nm. Additionally, the AgNCs exhibited a quazi-spherical shaped internal structure, which is expected. The TEM and SAED images in Figure 2 (d) (insert) both show lattice fringes, confirming that the particles are crystallized.

The FTIR graph in Figure 3(a) displays noticeable peaks that represent the distinct fingerprints of the AgNCs. Prominent peaks are seen for various stretches of bonds in the FTIR analysis. The peak at 3319.76 cm^{-1}, represents N-H stretch, 2078.45 cm^{-1} is assigned to C-H stretching vibrations, and 1591.15 cm^{-1} corresponds to the stretching vibration of C=C bond. The peak at 1118.05 corresponds to C=O. 1392.54 cm^{-1} corresponds to C-C and C-N stretching, while 1118.05 cm^{-1} assigned to –C= bond, and 732.82 cm^{-1} and 614.75 cm^{-1} are for C-H out-of-plane bend and CH bending vibrations, respectively. These peaks are comparable to unique fingerprints of silver nanomaterial as compared to literature [22,23]. It was determined through the utilization of UV-visible spectroscopy that the prepared materials are nanoparticles. Figure 3 (b) shows the plot of the absorption spectrum and Tauc's plot obtained from the UV-Vis spectroscopic analysis of the AgNCs over a range of 200 to 800 nm. The optical band gap energy (Eg) of the AgNCs can be obtained from the Tauc plot or calculated using Tauc's equation [24] which illustrates the relationship between the absorption coefficient and the incident photon energy of the material. The Tauc's equation is expressed as:

$$\alpha h\nu = A(h\nu - Eg)n \quad (1)$$

where α is the absorption coefficient, hν is the photon energy, A is a constant, Eg is the optical band gap, and n is a value that varies depending on the type of the electronic transition causing the absorption (n = ½ for direct transitions and n = 2 for indirect transitions). The band gap obtained from the Tauc plot for the AgNCs was 3.98 eV. This value confirms that the material exhibits good optical characteristics and will absorb in the UV-Vis range [18,25].

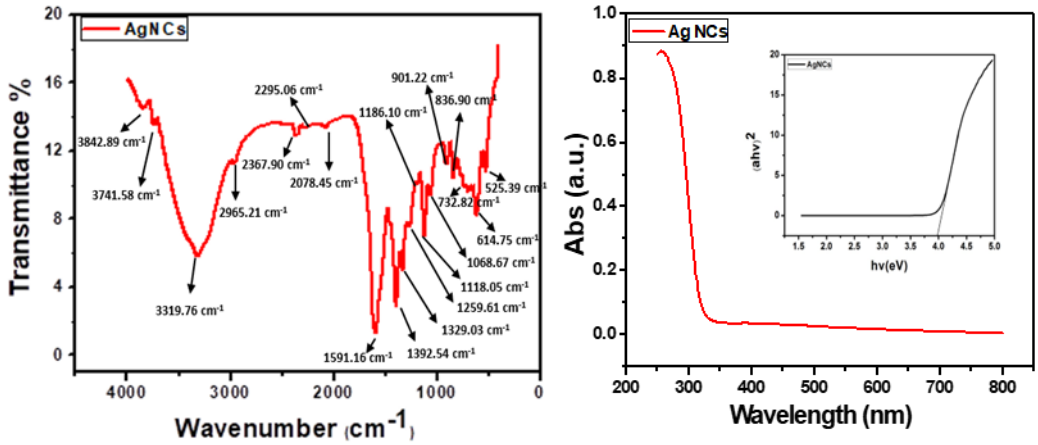

Figure 3. (a) FTIR (b) UV-Vis depicting the absorption spectrum and bandgap from the Tauc plot.

The crystal structure of the synthesized silver nanoparticles was confirmed by using the PANanalytical XRD equipment for X-ray diffraction experiments, and the High Score program for analysis. The XRD analysis result with the diffraction pattern is shown in Figure 4.

 doi:10.20944/preprints202505.1547.v1

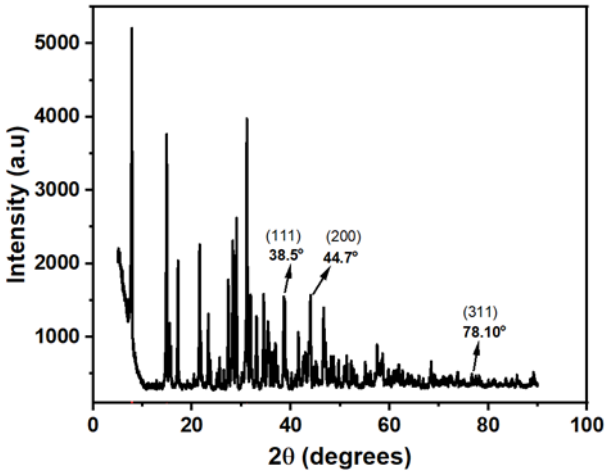

Figure 4. X-ray diffraction pattern.

The diffraction pattern of the powdered AgNCs shows sharp and well-defined diffraction peaks at 2θ = 38.5°, 44.7°, and 78.1°, which can be assigned to the (111), (200), and (311) reflections of the face-centered cubic (FCC) structure of pure metallic silver, respectively. This diffraction pattern is consistent with JCPDS File No 04-0783 and the literature report [26–28]. The produced silver nanoparticles' outstanding crystallinity is confirmed by these distinct, strong peaks in the diffraction pattern.

Figure 5 (a) to (d) show the small angle x-ray scattering (SAXS) analysis which was used to probe the internal composition of the synthesized nanoparticles, and they show the internal structure (a), the size distribution by number (b), and the size distribution by intensity (c), and the size distribution by volume (d), respectively. As observed in these figures, most of the particles appear at 1.7 nm radius (b) with a maximum diameter of 17 nm (a). The nanoparticles showed a maximum size distribution by intensity at 13.5 nm (c), and they also exhibited a spherically shaped internal structure (a), which is expected. The large number of small particles of 2 to 8 nm of particularly advantageous in increasing the surface area of the interaction layer by adhering reactant pathogen species to the layer.

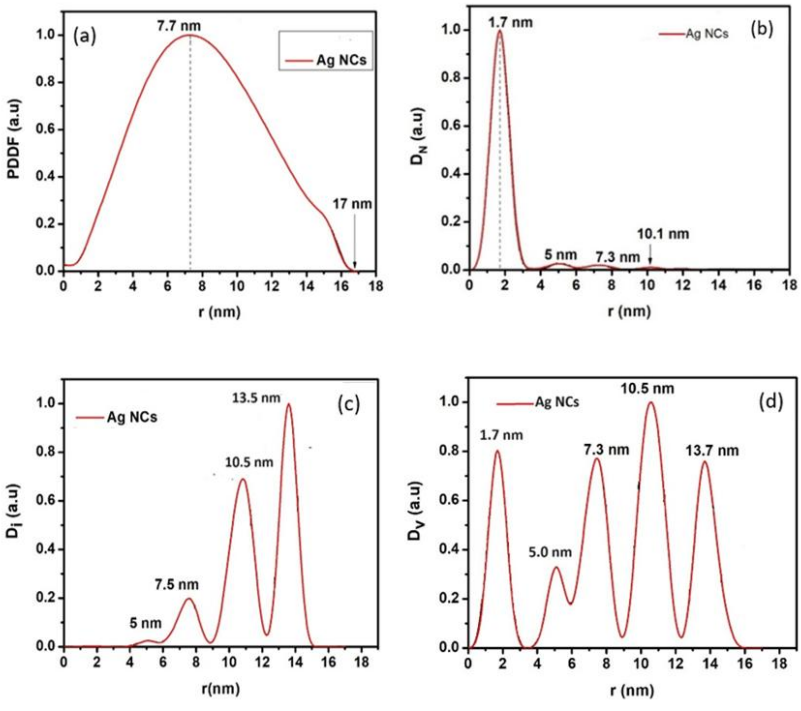

 doi:10.20944/preprints202505.1547.v1

Figure 5. Small angle X-ray diffraction analysis showing (a) internal structure (b) size distribution by number (c) size distribution by intensity, and (d) size distribution by volume.

3.2. Analytical Application of the Immunosensor

The immunosensor development steps were characterized using CV in 10 nM PBS of pH 7.4 in the potential window -1.0 to 1.0 and at a scan rate of 50 mV/s. Figure 6 shows the CV plots of the bare GCE, GCE|AgNC, GCE|AgNC|Ab, and GCE|AgNC|Ab|BSA. The bare GCE in Figure 6 shows no response. When AgNCs were introduced on the bare GCE, there was a significant amplification of the signal with prominent peaks at 0.25 V, and -0.125 V, which are associated with the oxidation of Ag from Ag^0 to Ag+ and its reduction from Ag+ back to Ag^0. Thus, the GCE|AgNC possesses a significantly higher surface area compared to the GCE. This increased surface area allows for a greater number of antibodies to be immobilized on the electrode surface.

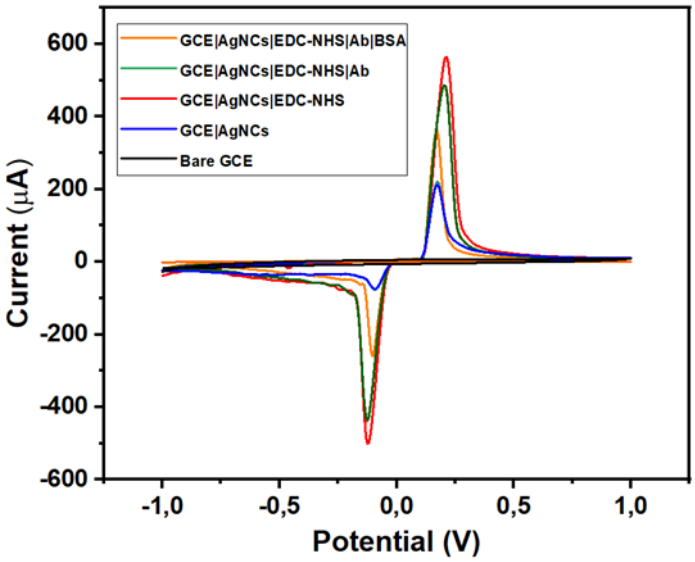

Figure 6. Cyclic voltammetry for the immunosensor fabrication steps.

More immobilized antibodies lead to more binding events with the target analyte, resulting in a stronger signal as seen with GCE|AgNC|Ab. EDC and NHS activate carboxyl groups (COOH) on the nanomaterial surface. This activation creates NHS esters that can readily react with the amine group ($-NH_2$) present in the antibody molecules, forming stable covalent amide bonds. When further modified with the EDC-NHS, a significant current increase is observed. EDC-NHS coupling promotes a more favourable orientation of the antibody on the surface, maximizing its antigen-binding capacity and thus the signal. EDC-NHS chemistry enables efficient and stable immobilization of a large number of functional antibodies [29]. A slight decrease in the current response is seen in GCE|AgNC|Ab to show that the antibody has been effectively immobilized on the surface of the electrode, thereby creating some resistance to the flow of electrons. After Ab is immobilized, there will still be uncovered areas on the electrode surface that could attract and bind other proteins or molecules present in the sample [29]. These non-specifically bound molecules can hinder the access of the target PSA antigen to the immobilized Ab, reducing the number of specific binding events and thus the signal. Therefore, BSA is used to block these remaining active sites on the electrode surface and effectively prevent other proteins in the sample from binding non-specifically. This is possible because BSA molecules are large and can cover the surface effectively, preventing other proteins or molecules from binding non-specifically [12]. This guarantees that the specific binding of PSA to the Ab is mainly responsible for any subsequent rise in signal current, and not the non-specific interactions. [30]. Because BSA is an insulator, it is therefore expected that the current response will diminish when it is immobilized on the electrode surface of the manufactured immunosensor,

 doi:10.20944/preprints202505.1547.v1

GCE|AgNC|Ab|BSA. This reaction is crucial as it confirms that BSA, a blocking agent, has been successfully immobilized on the electrode surface. When a sample containing PSA is introduced, the PSA molecules bind non-specifically to the capture antibodies. The blocked non-specific sites ensure that only PSA binds to the sensor, reducing background noise and improving the accuracy of the detection [13]. This binding event causes a measurable change in the sensor's properties which can alter the electrical signal, which is then measured using techniques like voltammetry. The decrease in current response observed in GCE|AgNC|Ab|BSA|PSA results from the resistance in electron transfer caused by the antibody capture of PSA for 10 ng/mL of PSA introduced in the buffer. This is because the core of the immunosensor is the specific interaction between the immobilized antibody on the sensor surface and the target antigen. Therefore, as PSA binds to Ab on the sensor surface, this binding event modulates the properties of the sensor interface in a way that reduces the peak current, allowing for the detection and quantification of PSA based on the magnitude of the signal decrease [29].

3.2.1. Stability, Reproducibility, and Selectivity

To study the stability of the prepared immunosensor, the current response was assessed by SWV in 10 mM PBS after one day, five days, seven days, ten days, and fourteen days of storage at 4 °C. The current response was observed as 100% after day one, 99.85% after day five, 99.42% on day seven, 99.13% on day ten, and 98.26% by day fourteen. From these results, the current response after fourteen days of storage decreased by only 1.74% (Figure 7 (a). This marginal current decrease confirms good stability of (98.26%). To investigate the sensor's selectivity, the interfering agents introduced were glucose, urea, L-cysteine, and alpha-methyl acyl-CoA racemases (AMACR). The sensor GCE|AgNC|Ab|BSA|PSA was run in 10 mM PBS of pH 7.4 in the presence of 5 ng/mL of the interfering species. The immunosensor only responded significantly to PSA. The immunosensor exhibited reasonable selectivity in the presence of these interferents as the current response produced by most of the interferents was less than 15%, with glucose alone at 38% (Figure 7 (b)). The reproducibility of the proposed immunosensor was interrogated by measuring the current response of 10 ng/ml of PSA using four different immunosensors prepared from different electrodes under the same experimental conditions. A relative standard deviation (RSD) of 5% was calculated for the measurements, confirming that the proposed method was repeatable and analytically significant. In summary, these results show that the fabricated immunosensor produced overall good stability, reproducibility, and selectivity.

 doi:10.20944/preprints202505.1547.v1

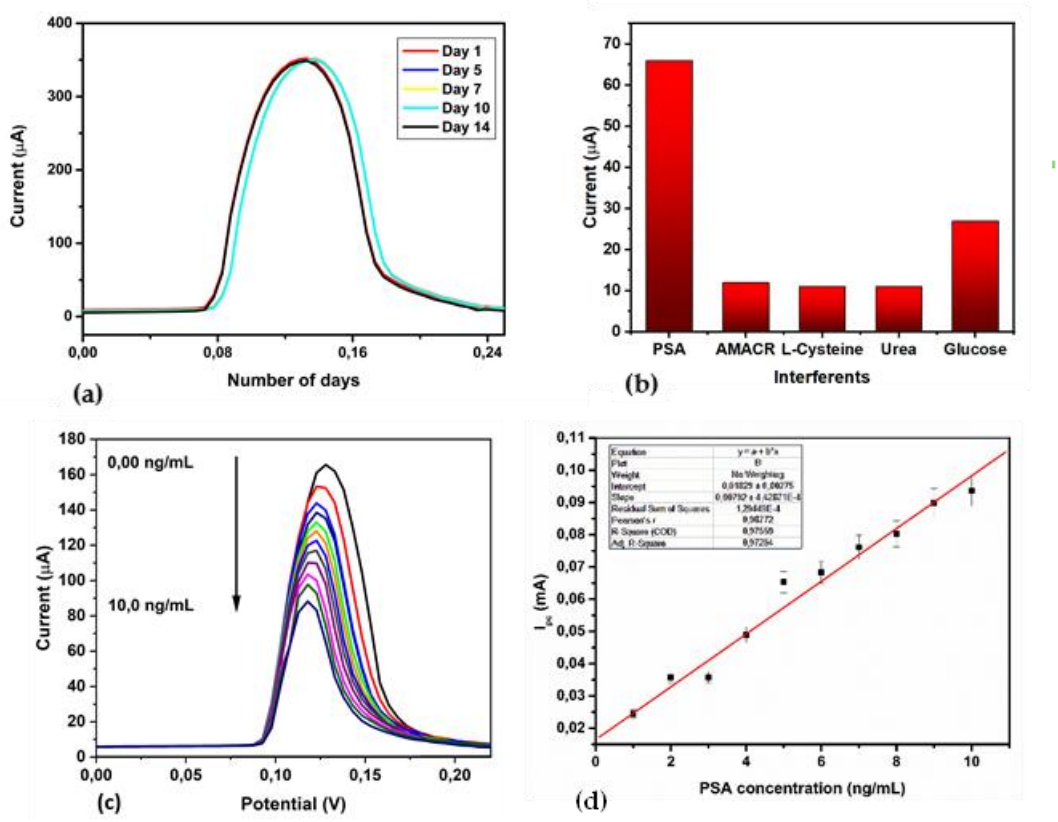

Figure 7. (a) SWV studies of the immunosensor studied over 14 days (b) interference studies of the constructed immunosensor in 10 mM PBS containing 5 ng/mL of the interferent species (c) SWV of detection studies of immunosensor in 10 mM PBS at increasing concentrations of analyte from 1.0 - 10.0 ng/mL (d) Linear calibration curve. .

3.2.2. Application in the Detection of PSA

For the detection studies, increasing concentrations of the analyte (PSA) from 1 to 10 ng/mL were added to a glass vial containing 10 mM PBS at pH 7.4 and transduced using SWV at a scan rate of 50 mV/s in the potential window of -1.0 to 1.0 V. The signal change was monitored with respect to the analyte concentrations as shown in Figure 7 (c). The higher concentrations of PSA lead to more binding on the sensor surface. This in turn results in a greater blockage of the electrode surface and a more significant impedance to the transfer of electrons on the surface of the sensor probe. The resultant decrease in current observed showed inverse proportionality to the concentration of PSA, which is reflected as a decrease in the overall signal response of the sensor. That is, the higher the PSA concentration, the larger the decrease in the signal compared to the baseline due to the capture of more PSA by its antibody in CGE|AgNC|Ab|BSA|PSA as seen in Figure 7 (c) and the linear calibration curve in Figure 7 (d). Over a concentration range of 1.0 to 10.0 ng/mL, the limit of detection (LOD) was calculated to be 1.14 ng/mL, with a sensitivity of 0.0079 (±0.00044) µA/(ng/mL) and a correlation coefficient (R^2) of 0.9877. The fabricated immunosensor in this investigation and others documented in the literature for PSA detection are compared in Table 1. The proposed PSA immunosensor reported in this study compares favourably to those reported in other studies in terms of linear range and limit of detection. It also exhibits promise in that it can be used for the diagnosis of prostate cancer in its early stages within the typical range of PSA concentrations of >4.0 ng/mL [31].

 doi:10.20944/preprints202505.1547.v1

Table 1. Comparison with PSA immunosensors that have already been published.

Immunosensor / electrode material	Detection method	Linear range (ng/mL)	LOD (ng/mL)	Ref.
BSA/Anti-PSA/PTH/GQD/MG /SPE	DPV	0.0125-1.0, 1.0-80.0	0.005	32
AuNPs-poly(FFP-AM)-RGO/AuE	DPV	0.01-110	0.001	33
SPE/AuNP//Anti-body/BSA	DPV	1.0-8.0	0.55	34
GCE/AgNP/Ab/BSA	CV	2.5-11	$1.7x10^{-1}$	18
(MoS_2@Cu_2O)-Au nanocomposite	L-SAW	0.2-5	0.076	35
MWCNTs	EIS	0 – 500	1.18	36
3D-GR-Au[a] / GCE	CV, DPV	0-10	0.59	37
Pipette-tip type biosensor	Fluorescence	0-10	1.2	38
GCE/AgNC/EDC-NHS/Ab/BSA	SWV	1-10	1.14	This work

The advantage of the proposed sensor developed is not only its efficacy for application in the detection of PSA, but it can be deployed in futuristic silicon photonic biosensor receptor layer for other biomarkers detection [17,18]. The proposed futuristic sensor is optical and noise-free, can be scaled down to micro and nano dimensions. Furthermore, it can be produced as a lab-on-a-chip device at commercial scale at a low cost. This proposed design also addresses the challenge of currently available ELISA tests used in clinical settings that require expensive equipment and highly trained staff. This proposed PSA diagnostic method is simple, affordable, user-friendly, and doesn't need a huge investment in highly trained staff, costly equipment, or a lot of space.

The schematic design of the proposed immunosensor is shown in Figure 8.

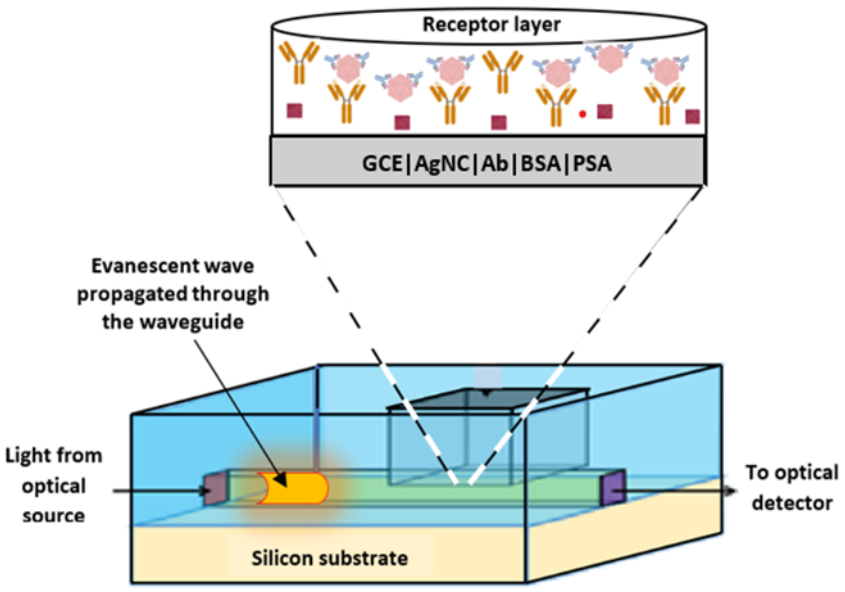

Figure 8. Schematic design of the proposed silicon photonic on-chip immunosensor with an optical source, evanescent-based waveguide propagation with etched bio-interaction cavity, and optical detector.

The sensor chip's etched bio-interaction receptor cavity is connected to a straight silicon oxide waveguide on a silicon substrate. An evanescent wave makes up around one-third of the wave that passes through the waveguide. This wave comes from the optical source and interacts with the sample analyzer in the carved cavity's bio-interaction region. The highly sensitive receptor later, which in this case has been modified for selective detection of PSA antigens, can provide an amplified signal of several orders of magnitude in response to the change in optical signal detected and

 doi:10.20944/preprints202505.1547.v1

processed by an optical detector and adjoining signal processing circuitry, all of which can be integrated on the same chip.

4. Conclusions

In this study, an immunosensor was developed for antigen detection using silver nanocrystals as an electrode-enhancement material. The immunosensor developed achieved a low limit of detection of 1.14 ng/mL, showed good stability and reproducibility, and was selective in the presence of interferent species. By integrating a receptor cavity interaction layer, an optical source, a waveguide, and an array of detectors all on-chip, this proposed design may be used in the future to create a new generation of silicon photonic microchip devices that can detect a range of analytes.

Author Contributions: Conceptualization, Timothy Okhai, Usisipho Feleni and Lukas Snyman; Data curation, Timothy Okhai; Formal analysis, Timothy Okhai; Funding acquisition, Timothy Okhai; Investigation, Timothy Okhai; Methodology, Timothy Okhai, Kefilwe Mokwebo and Marlon Oranzie; Project administration, Timothy Okhai; Resources, Lukas Snyman; Software, Timothy Okhai; Supervision, Usisipho Feleni and Lukas Snyman; Validation, Marlon Oranzie, Usisipho Feleni and Lukas Snyman; Visualization, Lukas Snyman; Writing – original draft, Timothy Okhai; Writing – review & editing, Kefilwe Mokwebo, Marlon Oranzie, Usisipho Feleni and Lukas Snyman.

Funding: This research was supported in part by the National Research Foundation of South Africa, Key International Collaboration Grant (KIC 69798), and the Department of Higher Education and Training (DHET) Grant administered by the Tshwane University of Technology, South Africa. Additional support was received from the UNISA, South Africa.

Institutional Review Board Statement: The study was conducted in accordance with the Declaration of Helsinki and approved by the SOE Ethics Review Committee of THE UNIVERSITY OF SOUTH AFRICA (protocol code 2019/CSET_SOC/TAO/001 and date of approval 26/09/2019).

Informed Consent Statement: Not applicable.

Data Availability Statement: No new data were created or analyzed in this study. Data sharing is not applicable to this article.

Acknowledgements: Special acknowledgement and thanks Dr Azeez Olayiwola Idris for his role in the synthesis and characterization of the nanomaterials used in this work. The iNanoWS Laboratory at UNISA, South Africa is also acknowledged and thanked for supporting the experimental work.

Conflicts of Interest: The authors declare no conflict of interest. The funders had no role in the design of the study; in the collection, analyses, or interpretation of data; in the writing of the manuscript; or in the decision to publish the results.

References

1. Cancer Center. CA-125 Blood Test: Cancer Antigen 125 Normal Range & High. Available online: https://www.cancercenter.com/cancer-types/ovarian-cancer/diagnosis-and-detection/ca-125-test (accessed on 9 April 2025).
2. De Gruyter. Quantification of the Lung Cancer Tumor Marker CYFRA 21-1 Using Protein. Available online: https://www.degruyter.com/document/doi/10.1515/cclm-2023-0795/html (accessed on 9 April 2025).9 April 2025).
3. American Cancer Society. Prostate Cancer Screening Tests. Available online: https://www.cancer.org/cancer/types/prostate-cancer/detection-diagnosis-staging/tests.html (accessed on 9 April 2025).
4. Alarfaj, N.A.; El-Tohamy, M.F.; Oraby, H.F. New Immunosensing-Fluorescence Detection of Tumor Marker Cytokeratin-19 Fragment (CYFRA 21-1) Via Carbon Quantum Dots/Zinc Oxide Nanocomposite. Nanoscale Res. Lett. 2020, 15, 12. Available online: https://link.springer.com/article/10.1186/s11671-020-3247-9 (accessed on 10 February 2025).
5. Kondo, K. Alpha-Fetoprotein: Diagnostic and Prognostic Insights in Liver Disease and Cancer. J. Preg. Neonatal Med. 2024, 8, 223. Available online: https://www.alliedacademies.org/articles/alphafetoprotein-diagnostic-and-prognostic-insights-in-liver-disease-and-cancer-31045.html (accessed on 10 February 2025).
6. Barlow, M.; Down, L.; Mounce, L.T.A.; Funston, G.; Merriel, S.W.D.; Watson, J.; Abel, G.; Kirkland, L.; Martins, T.; Bailey, S.E.R. The Diagnostic Performance of CA-125 for the Detection of Ovarian Cancer in Women from Different Ethnic Groups: A Cohort Study of English Primary Care Data. J. Ovarian Res. 2024,

 doi:10.20944/preprints202505.1547.v1

17, 173. Available online: https://ovarianresearch.biomedcentral.com/articles/10.1186/s13048-024-01490-5 (accessed on 10 February 2025).
7. Hariri, M.; Alivirdiloo, V.; Ardabili, N.S.; Gholami, S.; Masoumi, S.; Mehraban, M.R.; Alem, M.; Hosseini, R.S.; Mobed, A.; Ghazi, F.; Alipourfard, I. Biosensor-Based Nanodiagnosis of Carcinoembryonic Antigen (CEA): An Approach to Classification and Precise Detection of Cancer Biomarker. BioNanoScience 2024, 14, 429-446. Available online: https://link.springer.com/article/10.1007/s12668-023-01250-7 (accessed on 10 February 2025).
8. Merriel, S.W.D.; Pocock, L.; Gilbert, E.; Creavin, S.; Walter, F.M.; Spencer, A.; Hamilton, W. Systematic Review and Meta-Analysis of the Diagnostic Accuracy of Prostate-Specific Antigen (PSA) for the Detection of Prostate Cancer in Symptomatic Patients. BMC Med. 2022, 20, 54. Available online: https://bmcmedicine.biomedcentral.com/articles/10.1186/s12916-021-02230-y (accessed on 10 February 2025).
9. Kirlangiç, I.A.; Üner, G.; Kara, P.; Kirmizibayrak, P.B.; Ertaş, F.N. Development of Transition Metal Oxide Platforms for Aptasensing of PSA in Cell Cultures. Anal. Bioanal. Chem. 2024, 416, 6421-6435. Available online: https://link.springer.com/article/10.1007/s00216-024-05529-w (accessed on 10 February 2025).
10. Rajarathinam, T.; Jayaraman, S.; Kim, C.-S.; Lee, J.; Chang, S.-C. Portable Amperometric Biosensor Enhanced with Enzyme-Ternary Nanocomposites for Prostate Cancer Biomarker Detection. Biosensors 2024, 14, 623. Available online: https://www.mdpi.com/2079-6374/14/12/623 (accessed on 10 February 2025).
11. Oliveira, N.; Costa-Rama, E.; Viswanathan, S.; Delerue-Matos, C.; Pereira, L.; Morais, S. Label-Free Voltammetric Immunosensor for Prostate Specific Antigen Detection. Biosensors 2020, 10, 1-14. Available online: https://core.ac.uk/download/pdf/232112986.pdf (accessed on 10 February 2025).
12. Yan, L.; Xu, S.; Xi, F. Disposal Immunosensor for Sensitive Electrochemical Detection of Prostate-Specific Antigen Based on Amino-Rich Nanochannels Array-Modified Patterned Indium Tin Oxide Electrode. Nanomaterials 2022, 12, 3810. https://doi.org/10.3390/nano12213810.
13. Presnova, G.V.; Presnov, D.E.; Ulyashova, M.M.; Tsiniaikin, I.I.; Trifonov, A.S.; Skorb, E.V.; Krupenin, V.A.; Snigirev, O.V.; Rubtsova, M.Y. Ultrasensitive Detection of PSA Using Antibodies in Crowding Polyelectrolyte Multilayers on a Silicon Nanowire Field-Effect Transistor. Polymers 2024, 16, 332. https://doi.org/10.3390/polym16030332.
14. Police Patil, A.V.; Chuang, Y.-S.; Li, C.; Wu, C.-C. Recent Advances in Electrochemical Immunosensors with Nanomaterial Assistance for Signal Amplification. *Biosensors* **2023**, *13*, 125. Available online: https://www.mdpi.com/2079-6374/13/1/125 (accessed on 10 February 2025).
15. Walgama, C.; Raj, N. Silver Nanoparticles in Electrochemical Immunosensing and the Emergence of Silver–Gold Galvanic Exchange Detection. Chem. Commun. 2023, 59, 75. Available online: https://pubs.rsc.org/en/content/articlelanding/2023/cc/d3cc02561f (accessed on 10 February 2025).
16. Rodrigues, A.S.; Batista, J.G.S.; Rodrigues, M.Á.V.; Thipe, V.C.; Minarini, L.A.R.; Lopes, P.S.; Lugão, A.B. Advances in Silver Nanoparticles: A Comprehensive Review on Their Potential as Antimicrobial Agents and Their Mechanisms of Action Elucidated by Proteomics. Front. Microbiol. 2024, 15, 1440065. Available
17. **Okhai, T.A.; Idris, A.O.; Feleni, U.; et al.** Nanomaterial-Enhanced Receptor Technology for Silicon On-Chip Biosensing Application. *Biosensors—Current and Novel Strategies for Biosensing*; IntechOpen, 2021. Available online: https://dx.doi.org/10.5772/intechopen.94249 (accessed on 23/04/2025).
18. Okhai, T.A.; Idris, A.O.; Feleni, U.; Snyman, L.W. Futuristic Silicon Photonic Biosensor with Nanomaterial Enhancement for PSA Detection. *Photonics* 2024, *11*, 97. https://doi.org/10.3390/photonics11010097
19. Li, H.; Xia, H.; Wang, D.; Tao, X. Simple Synthesis of Monodisperse, Quasi-spherical, Citrate-Stabilized Silver Nanocrystals in Water. *Langmuir* **2013**, *29*, 5074–5079. https://doi.org/10.1021/la400214x.
20. Völkle, C.M.; Gebauer, D.; Colfen, H. High-resolution insights into the early stages of silver nucleation and growth. *Faraday Discuss.* **2015**, *179*, 59–77. DOI: 10.1039/C4FD00269E.
21. Javed, R.; Zia, M.; Naz, S.; Aisida, S.O.; ul Ain, N.; Ao, Q. Role of capping agents in the application of nanoparticles in biomedicine and environmental remediation: recent trends and future prospects. *J. Nanobiotechnol.* **2020**, *18*, 172. DOI: 10.1186/s12951-020-00704-4.
22. Kalpana, D.; Han, J.H.; Park, W.S.; Lee, S.M.; Wahab, R.; Lee, Y.S. Green biosynthesis of silver nanoparticles using Torreya nucifera and their antibacterial activity. Arab. J. Chem. 2019, 12, 1722–1732. https://doi.org/10.1016/j.arabjc.2014.08.016
23. Devara J, Kumari P, Aarti C, and Renganathan A. Synthesis and characterization of Silver nanoparticles using cannon ball leaves and their cytotoxic activity against MCF-7 line. Nanocomposites. 2013; 598328. DOI: 101155/2013/598328
24. Al-Khedhairy, A.A.; Wahab, R. Silver Nanoparticles: An Instantaneous Solution for Anticancer Activity against Human Liver (HepG2) and Breast (MCF-7) Cancer Cells. *Metals* 2022, *12*, 148. https://doi.org/10.3390/met12010148
25. Nilavukkarasi, M.; Vijayakumar, S.; Kumar, S.P. Biological Synthesis and Characterization of Silver Nanoparticles with *Capparis zeylanica* L. Leaf Extract for Potent Antimicrobial and Anti-Proliferation Efficiency. *Mater. Sci. Energy Technol.* **2020**, *3*, 371–376. doi:10.1016/j.mset.2020.02.008.

 doi:10.20944/preprints202505.1547.v1

26. Harisha, K.S.; Parushuram, N.; Ranjana, R.; Martis, L.J.; Narayana, B.; Sangappa, Y. Characterization and Antibacterial 595 Properties of Biogenic Spherical Silver Nanoparticles. Mater. Today Proc. 2020, 37, 254–263://doi.org/10.3390/chemosensors9040085
27. Huong, V.T.L.; Thang, N.N. Green Synthesis, Characterization and Antibacterial Activity of Silver Nanoparticles Using 600 Sapindus Mukorossi Fruit Pericarp Extract. Mater. Today Proc. 2020, 37, 254– 601 263. https://doi.org/10.1016/j.matpr.2020.10.015
28. Lava, M.B.; Muddapur, U.M.; Basavegowda, N.; More, S.S.; More, V.S. Characterization, Anticancer, Antibacterial, Anti- 597 Diabetic and Anti-Inflammatory Activities of Green Synthesized Silver Nanoparticles Using Justica Wynaadensis Leaves 598 Extract. Mater. Today Proc. 2020, 37, 254–263. https://doi.org/10.1016/j.matpr.2020.10.04
29. Patel, M.; Agrawal, M.; Srivastava, A. Signal Amplification Strategies in Electrochemical Biosensors via Antibody Immobilization and Nanomaterial-Based Transducers. *Mater. Adv.* **2022**, *3*, 8864–8885. doi:10.1039/D2MA00427E.
30. Ahirwar, R.; Bariar, S.; Balakrishnan, A.; Nahar, P. BSA Blocking in Enzyme-Linked Immunosorbent Assays Is a Non-Mandatory Step: A Perspective Study on Mechanism of BSA Blocking in Common ELISA Protocols. *RSC Adv.* **2015**, *5*, 20750–20760. doi:10.1039/C5RA20750A.
31. Hildebrandt, B. What are Normal PSA Levels by Age? Men's Hormonal Health. June 23, 2019. Online. Accessed on 10 April 2025. Available from: https://www.menshormonalhealth.com/psa-test-results.html.
32. Cotchim S, Kongkaew S, Thavarungkul P, Kanatharana P, Limbut W. An Unlabeled Electrochemical Immunosensor Uses Poly(thionine) and Graphene Quantum Dot-Modified Activated Marigold Flower Carbon for Early Prostate Cancer Detection. Biosensors (Basel). 2024 Dec 2;14(12):589. doi: 10.3390/bios14120589. PMID: 39727854; PMCID: PMC11674062.
33. Han, B.; Chen, Y.; Wang, H.; Zhao, W.; Hu, Y.; Guo, Y.; Yan, J.; Jia, S. A Label-free Electrochemical Immunosensor Based on Gold Nanoparticles-poly(ferriporphyrin-co-acrylamide)-reduced Graphene Oxide and the Application in Prostate Specific Antigen Detection. Electrochemistry 2024, 92, 027006. https://doi.org/10.5796/electrochemistry.23-00104
34. Cândido, Thaís & Pereira, Arnaldo & Silva, Daniela & Ferreira, Lucas & Tarley, César. (2024). Development of a screen-printed electrochemical immunosensor modified with gold nanoparticles for prostate-specific antigen (PSA) detection. Journal of Solid State Electrochemistry. 29. 1173-1185. 10.1007/s10008-024-05939-x.
35. Yu, Y.; Xie, H.; Zhou, T.; Zhang, H.; Lu, C.; Tao, R.; Tang, Z.; Luo, J. Real-Time and Ultrasensitive Prostate-Specific Antigen Sensing Using Love-Mode Surface Acoustic Wave Immunosensor Based on MoS2@Cu2O-Au Nanocomposites. Sensors 2024, 24, 7636. https://doi.org/10.3390/s24237636
36. Ji, S.; Lee, M.; Kim, D. Detection of Early Stage Prostate Cancer by Using a Simple Carbon Nanotube@Paper Biosensor. 646 Biosens. Bioelectron. 2018, 102, 345–350, doi:10.1016/j.bios.2017.11.035.
37. Jang, H.D.; Kim, S.K.; Chang, H.; Choi, J.-W. 3D Label-Free Prostate Specific Antigen (PSA) Immunosensor Based on Graphene–Gold Composites. Biosens. Bioelectron. 2015, 63, 546–551, doi:10.1016/j.bios.2014.08.008.
38. Takano, E.; Shimura, N.; Ujima, Y.; Sunayama, H.; Kitayama, Y.; Takeuchi, T. Highly Sensitive Fluoro-Immunosensing for Biomarker Detection Using an Automatic Pipette Tip-Type Biosensing System. ACS Omega 2019,4 1487-1493. https://doi.org/10.1021/acsomega.8b02850